# Design of Broadband Aperture-Coupled Stacked Microstrip Antennas using Second-Order Filter Theory

Nieves García-Alcaide, Armando Fernández-Prieto, *Senior Member, IEEE,* Rafael R. Boix, *Member, IEEE,* Vicente Losada, Jesús Martel, *Senior Member, IEEE,* and Francisco Medina, *Fellow, IEEE*

***Abstract*—In this paper the authors propose a lumped circuit methodology for the design of broadband stacked microstrip patch antennas fed through an aperture. First, an equivalent circuit (EC) is introduced for the antenna. The EC consists of an LC series resonator modelling the feed plus two capacitively coupled LC parallel resonators accounting for the radiating patches. Then, a de-embedding procedure based on total least squares method is introduced to determine all the parameters of the antenna EC. Second, the circuit stage modelling the patches is designed as a second-order Chebyshev filter based on coupled resonators. Since the standard Chebyshev approach leads to circuit parameters that cannot be physically obtained in practice, a modified second-order quasi-Chebyshev design is presented, which can be physically implemented by stacking one conventional rectangular patch above one rectangular patch with both inner and meandering slots. The proposed methodology is used to design an antenna with over 30% bandwidth at a center frequency of 5.57 GHz. A prototype has been fabricated and measured, and good agreement has been found between simulations and experiments.**

***Index Terms*—Microstrip antennas, aperture coupled antennas, broadband antennas, filtering theory**

## I. Introduction

ALTHOUGH there are different ways to feed microstrip patch antennas, aperture-coupled feeding is probably the most convenient way because it makes it possible to use a thick low-permittivity substrate for the patch antenna and a thin high-permittivity substrate for the feeding microstrip line, because it avoids interference between the fields radiated by the antenna to the front half-space and the fields radiated by the open-ended microstrip line to the back half-space, and because it provides several degrees of freedom to optimize the matching of the antenna [1]–[3]. Aperture-coupled microstrip antennas have a relatively small bandwidth, but this problem can be solved by stacking two patches as shown in [4], where bandwidths close to 25% have been achieved. In fact, Targonsky et al. report on bandwidths close to 70% if the stacked patches are fed by a resonant aperture, but this huge bandwidth is achieved at the expense of a large front-to-back radiation ratio due to the resonant aperture back radiation [5]. All through the years the basic configuration of aperture-coupled microstrip antennas has evolved to enable new applications such as dual-frequency operation [6], broadband dual-polarization operation [7], dual-band dual-polarization operation with filtering gain response [8], filtering response with high selectivity [9], etc.

In the last few years, the topic of filtering microstrip antennas has attracted many researchers. In some cases, the design of these antennas has been based on microwave coupled resonator filters in which the antenna radiator is the last-stage resonator of the filter [10]–[15]. As commented in the review paper by Mao et al. [16], a useful approach for filtering microstrip antenna design follows the coupling matrix theory of [17], based on computation of external quality factors and coupling coefficients. Since there is not output port in the filtering microstrip antenna, the extraction of circuit parameters for the radiating patch (last-stage resonator) has to rely on a lumped circuit model whose parameters are either extracted by means of numerical simulations [18] or obtained by means of closed-form expressions [19], [20]. Although the coupling matrix theory has been used to design antennas with different filtering responses (Chebyshev, quasi-elliptic, etc.) and different polarizations (linear and circular) in single and dual frequency bands [8], [18]–[22], the resulting bandwidth of the antennas is relatively small (usually below 10%) since coupling matrix theory is a narrowband theory which relies on the assumption that coupling coefficients are frequency independent, even though coupling coefficients do in fact depend on frequency [23]. An alternative approach in the design of filtering antennas is the so-called fusion method [16], in which band-stop responses are introduced at both sides of the passband by either incorporating transmission zeros in the feeding network or radiation nulls due to field interference between the feeding network and the patch antenna [9], [24]–[26].

In this paper second-order filter theory is used as a means to design broadband microstrip antennas consisting of two stacked patches which are aperture coupled to a microstrip

This work was supported by Grant PID2020-116739GB-I00 funded by MCIN/AEI/ 10.13039/501100011033, by Grant TEC2017-84724-P funded by MCIN/AEI/ 10.13039/501100011033 and "ERDF A way of making Europe", and by Contract EJ3-58 of the Spanish National System of Young Guarantee at the "Universidad de Sevilla". (*Corresponding author: Rafael R. Boix*)

N. García-Alcaide, A. Fernández-Prieto, R. R. Boix and F. Medina are with the Microwaves Group, Department of Electronics and Electromagnetism, College of Physics, Universidad de Sevilla, Avda. Reina Mercedes s/n, 41012, Seville, Spain (e-mails: nievesgar96@gmail.com, armandof@us.es, boix@us.es, medina@us.es).

V. Losada is with the Microwaves Group, Department of Applied Physics I, E.T.S. de Ing. Informática, Universidad de Sevilla, Av. Reina Mercedes, s/n, 41012, Seville, Spain (e-mail: losada@us.es).

J. Martel is with the Microwaves Group, Department of Applied Physics II, E.T.S. de Arquitectura, Universidad de Sevilla, Av. Reina Mercedes, s/n, 41012, Seville, Spain (e-mail: martel@us.es).

line. In this sense, the paper has some similarity with Ref. [20], where second-order filter theory is used as a means to design a broadband circularly polarized microstrip antenna. Although "rules of thumb" have been provided for the design of broadband microstrip antennas based on stacked patches (see [27] and references therein), the goal pursued in this paper is to provide a systematic design methodology based on filter theory for this type of antennas. In the paper an equivalent circuit (EC) is introduced for the studied antenna, which is made of an LC series stage accounting for the feed, and by two LC capacitively coupled parallel resonators accounting for the radiating patches. A total least squares approach [28], [29] is proposed to extract the electrical parameters of the EC from numerical simulations. Once the EC parameters are available, antenna dimensions are adjusted so that the circuit parameters match those of a quasi-Chebyshev response, which is derived as an evolution of the standard second-order Chebyshev filter based on the insertion loss method [30]. Since we are interested in antennas with large bandwidths above 20%, the lumped circuit approach is directly used in this paper rather than the coupling matrix approach, since this is only valid within the narrowband approximation [23]. A stacked patch microstrip antenna has been fabricated and measured with a fractional bandwidth of 32% and a center frequency of 5.57 GHz. Good agreement has been found between simulations and experiments, thus validating the proposed design methodology.

## II. Antenna design based on filter theory

### A. Microstrip antenna and equivalent circuit

Figs. 1(a) to (e) show the side view and the different metallization levels of the broadband multilayered microstrip antenna designed in this paper. The four layers of the substrate are assumed to have a thickness $h_i$ $(i = 1, \ldots, 4)$, a complex permittivity $\varepsilon_i = \varepsilon_0 \varepsilon_{r,i}(1 - \mathrm{j}\tan\delta_i)$ $(i = 1, \ldots, 4)$, and a permeability $\mu_0$. A feeding open-ended microstrip line (Fig. 1(e)) couples to a pair of stacked microstrip patches (Figs. 1(b) and (c)) through a non-resonant rectangular aperture (Fig. 1(d)) located in the ground plane of the microstrip line [1]. The lower stacked patch shown in Fig. 1(c) is a rectangular patch loaded with two inner slots close to the center of the patch, and with four meandering slots close to the corner of the patch. This particular geometry of microstrip patch, previously employed in [31] for dual-band and miniaturization applications, is employed in this case to narrow the current paths in the patch, and to increase the patch inductance. Note that whereas in [31] the inner and meandering slots were oriented perpendicularly to the current direction, in this paper the slots are oriented in the current direction to minimize the impact of the slots on the antenna performance. The inner and meandering slots are located so as to preserve the mirror symmetry of the patch with respect to the planes $x = 0$ and $y = 0$. The upper stacked patch is a standard rectangular patch.

Fig. 2 shows the equivalent circuit (EC) of the microstrip antenna shown in Figs. 1(a) to (e), where $Z_{\mathrm{in}}(\omega)$ is the input impedance at the plane $y = l_2 + s_2/2$ of the feeding microstrip line of Fig. 1(e). The LC series resonator directly connected

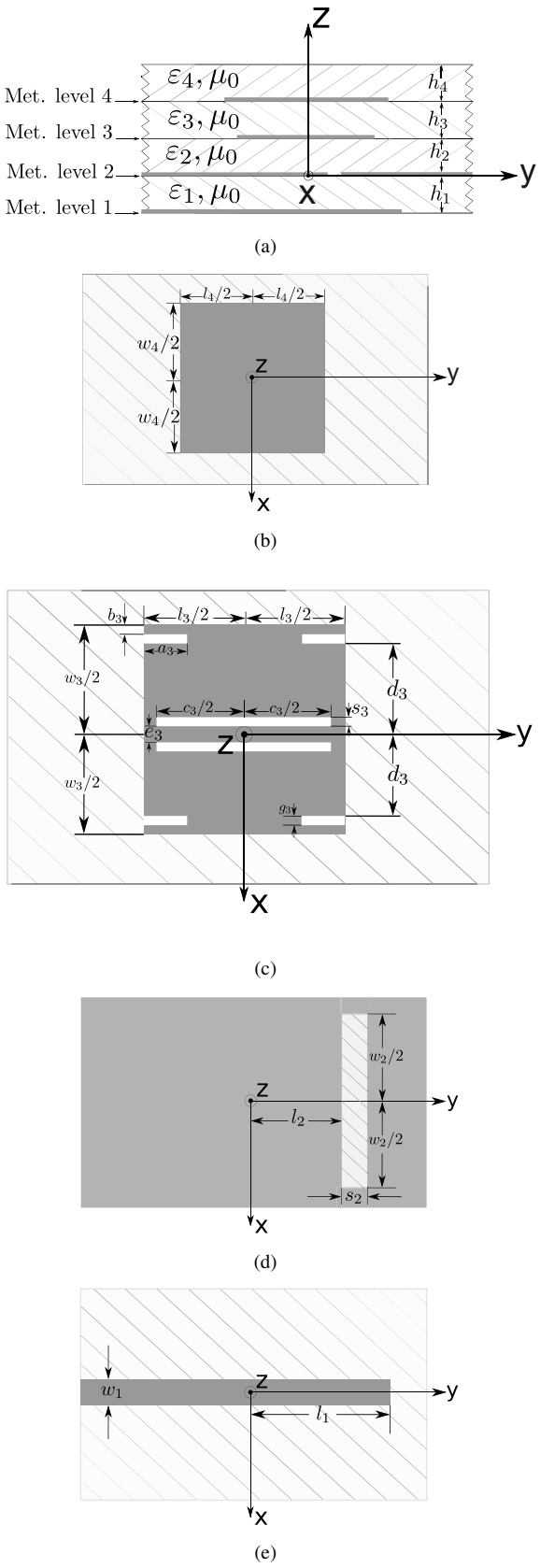


Fig. 1. Aperture-coupled microstrip antenna consisting of two stacked patches. (a) Side view. (b) Layout of the rectangular patch located at metallization level 4. (c) Layout of the rectangular patch with inner and meandering slots located at metallization level 3. (d) Layout of the ground plane rectangular aperture located at metallization level 2. (e) Layout of the feeding strip located at metallization level 1.

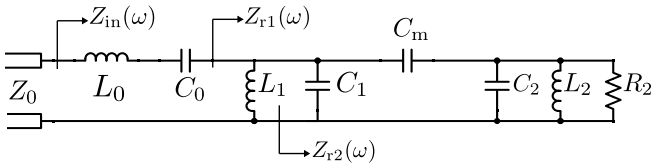


Fig. 2. Equivalent circuit of the aperture-coupled stacked microstrip antenna shown in Fig. 1.

to the feeding transmission line stands for the open-ended microstrip stub existing after the aperture. Since this open-ended stub is typically shorter than one quarter of the feeding line wavelength at the design center frequency [3], it can be modelled as an LC series resonator [30, Sect. 8.8]. The circuit parameters $L_0$ and $C_0$ not only depend on the stub length, $l_1 - l_2 - s_2/2$, but also depend on the aperture length $w_2$ and the aperture position with respect to the center of the patches, given by $l_2$. In fact, the role of the geometrical parameters $l_1$, $l_2$ and $w_2$ (and therefore, the role of $L_0$ and $C_0$) is to match the feeding microstrip line to the radiating patches in its whole operation frequency band [3]. The two LC parallel resonators in Fig. 2 stand for the radiating patches, which are strongly coupled by means of the coupling capacitance $C_{\rm m}$. And finally, the resistance $R_2$ accounts for radiation losses.

### *B. De-embedding of the equivalent circuit parameters*

In this paper the multilayered microstrip antenna drawn in Fig. 1 has been simulated by means of Momentum 3D Planar EM software [32], and the EC parameters of Fig. 2 have been computed so as to match the frequency response of the complex reflection coefficient of the antenna in its operating frequency band. In general, the retrieving of unknown parameters of lumped elements in ECs from simulated scattering parameters is not a trivial task. Costa et al. [33] suggest to use the information on the poles and zeros of the EC input impedance to ease the determination of the circuit parameters. However, in [33] this strategy is applied for the determination of ECs with a maximum of four lumped elements with unknown parameters. The EC of Fig. 2 is far more complicated than those presented in [33] since it contains eight lumped elements with unknown parameters, and therefore, we have followed a completely different strategy in the determination of the EC parameters.

Let $S_{11}(\omega)$ be the reflection coefficient at the plane $y = l_2 + s_2/2$ of the feeding microstrip line of Fig. 1(e) in a certain frequency band, which can be obtained by Momentum simulations. Then, the antenna input impedance, $Z_{\rm in}(\omega)$, can be obtained in that frequency band in terms of $S_{11}$ as shown below

$$Z_{\rm in}(\omega) = Z_0 \frac{1 + S_{11}(\omega)}{1 - S_{11}(\omega)}. \tag{1}$$

Since $Z_{\rm in}(\omega)$ is the input impedance of the EC of Fig. 2, it can be shown that $Z_{\rm in}(\omega)$ can be expressed as a rational function of $\omega$ given by

$$Z_{\rm in}(\omega) = \frac{{\rm j}N_{\rm e6}(\omega) + N_{\rm o5}(\omega)}{[\omega^5 + D_{\rm o3}(\omega)] + {\rm j}D_{\rm e4}(\omega)}, \tag{2}$$

where $N_{\rm e6}(\omega) = \alpha_6\omega^6 + \alpha_4\omega^4 + \alpha_2\omega^2 + \alpha_0$, $N_{\rm o5}(\omega) = \alpha_5\omega^5 + \alpha_3\omega^3 + \alpha_1\omega$, $D_{\rm o3}(\omega) = \beta_3\omega^3 + \beta_1\omega$ and $D_{\rm e4}(\omega) = \beta_4\omega^4 + \beta_2\omega^2$ are real polynomials of the real variable $\omega$. The complete characterization of the rational function of (2) for $Z_{\rm in}(\omega)$ requires the determination of the eleven unknown coefficients $\alpha_i$ $(i = 0, \ldots, 6)$ and $\beta_i$ $(i = 1, \ldots, 4)$. In order to compute those coefficients, we rewrite (2) as

$$\begin{aligned} Z_{\rm in}(\omega)\omega^5 =& {\rm j}N_{\rm e6}(\omega) + N_{\rm o5}(\omega) \\ & - Z_{\rm in}(\omega)[D_{\rm o3}(\omega) + {\rm j}D_{\rm e4}(\omega)], \end{aligned} \tag{3}$$

and we take the complex conjugate of (3), thus obtaining

$$\begin{aligned} Z^*_{\rm in}(\omega)\omega^5 =& -{\rm j}N_{\rm e6}(\omega) + N_{\rm o5}(\omega) \\ & - Z^*_{\rm in}(\omega)[D_{\rm o3}(\omega) - {\rm j}D_{\rm e4}(\omega)]. \end{aligned} \tag{4}$$

Now, we add (3) and (4) to obtain the equation

$$\begin{aligned} [Z_{\rm in}(\omega) + Z^*_{\rm in}(\omega)]\omega^5 =& 2N_{\rm o5}(\omega) - [Z_{\rm in}(\omega) + Z^*_{\rm in}(\omega)]D_{\rm o3}(\omega) \\ & - {\rm j}[Z_{\rm in}(\omega) - Z^*_{\rm in}(\omega)]D_{\rm e4}(\omega), \end{aligned} \tag{5}$$

which only involves real quantities (note $Z_{\rm in}(\omega)$ is a complex quantity). Also, we substract (3) and (4), and multiply the resulting equation by the imaginary unit j to yield

$$\begin{aligned} {\rm j}[Z_{\rm in}(\omega) - Z^*_{\rm in}(\omega)]\omega^5 =& -2N_{\rm e6}(\omega) - {\rm j}[Z_{\rm in}(\omega) - Z^*_{\rm in}(\omega)]D_{\rm o3}(\omega) \\ & + [Z_{\rm in}(\omega) + Z^*_{\rm in}(\omega)]D_{\rm e4}(\omega), \end{aligned} \tag{6}$$

which is also an equation only involving real quantities.

Eqns. (5) and (6) are real number equations satisfied by the real unknown coefficients $\alpha_i$ and $\beta_i$. If we oblige that these two equations are satisfied in a huge number of frequency values within the frequency interval for which $Z_{\rm in}(\omega)$ has been derived from (1) by means of Momentum simulations (we have checked that 200 sampling frequencies suffice in practice), we obtain an overdetermined system of linear equations for the unknowns $\alpha_i$ and $\beta_i$. Total least squares (TLS) method [28], [29] has been applied to the solution of this overdetermined system of linear equations. The use of TLS is convenient since the available values of $Z_{\rm in}(\omega)$ are not exact but extracted from approximate electromagnetic simulations, and therefore, are subjected to errors [28].

Once $\alpha_i$ and $\beta_i$ have been determined, standard circuit theory can be used in (2) to show that the circuit parameters $L_0$ and $C_0$ of Fig. 2 can be obtained as

$$L_0 = \lim_{\omega\to\infty} \frac{Z_{\rm in}(\omega)}{{\rm j}\omega} = \alpha_6 \tag{7}$$

$$C_0 = \lim_{\omega\to 0} \frac{1}{{\rm j}\omega Z_{\rm in}} = -\frac{\beta_1}{\alpha_0}. \tag{8}$$

Next, we define the impedance $Z_{\rm r1}(\omega)$ of Fig. 2 as

$$Z_{\rm r1}(\omega) = Z_{\rm in}(\omega) - {\rm j}\omega L_0 + \frac{\rm j}{\omega C_0}. \tag{9}$$

Using Fig. 2, it can be shown that $Z_{\rm r1}(\omega)$ can be expressed as a rational function of $\omega$ given by

$$Z_{\rm r1}(\omega) = \frac{{\rm j}N'_{\rm o3}(\omega) + N'_{\rm e2}(\omega)}{[\omega^4 + D'_{\rm e2}(\omega)] + {\rm j}D'_{\rm o3}(\omega)}, \tag{10}$$

where $N'_{\rm o3}(\omega) = \gamma_3\omega^3 + \gamma_1\omega$, $N'_{\rm e2}(\omega) = \gamma_2\omega^2$, $D'_{\rm e2}(\omega) = \delta_2\omega^2 + \delta_0$ and $D'_{\rm o3}(\omega) = \delta_3\omega^3 + \delta_1\omega$ are real polynomials

of the real variable $\omega$. The rationale used to determine the unknown coefficients $\alpha_i$ and $\beta_i$ by means of the TLS method is repeated to determine the seven unknown coefficients $\gamma_i$ ($i = 1, \ldots, 3$) and $\delta_i$ ($i = 0, \ldots, 3$). Once these coefficients are all known, the circuit parameter $L_1$ of Fig. 2 can be obtained as

$$L_1 = \lim_{\omega \to 0} \frac{Z_{\mathrm{r}1}(\omega)}{\mathrm{j}\omega} = \frac{\gamma_1}{\delta_0}. \tag{11}$$

Once again, the impedance $Z_{\mathrm{r}2}(\omega)$ of Fig. 2 is defined by means of the equation

$$\frac{1}{Z_{\mathrm{r}2}(\omega)} = \frac{1}{Z_{\mathrm{r}1}(\omega)} - \frac{1}{\mathrm{j}\omega L_1}, \tag{12}$$

and $1/Z_{\mathrm{r}2}(\omega)$ can be expressed by means of the rational function of $\omega$

$$\frac{1}{Z_{\mathrm{r}2}(\omega)} = \frac{\mathrm{j}N''_{\mathrm{o}3}(\omega) + N''_{\mathrm{e}2}(\omega)}{[\omega^2 + D''_{\mathrm{e}0}(\omega)] + \mathrm{j}D''_{\mathrm{o}1}(\omega)}, \tag{13}$$

where $N''_{\mathrm{o}3}(\omega) = \lambda_3\omega^3 + \lambda_1\omega$, $N''_{\mathrm{e}2}(\omega) = \lambda_2\omega^2$, $D''_{\mathrm{e}0}(\omega) = \xi_0$ and $D''_{\mathrm{o}1}(\omega) = \xi_1\omega$ are real polynomials of the real variable $\omega$. The TLS method can be applied once again to determine the five unknown coefficients $\lambda_i$ ($i = 1, \ldots, 3$) and $\xi_i$ ($i = 0, 1$) as in the case of (2) and (10). Once $\lambda_i$ and $\xi_i$ have been determined, the quantity $C_1 + C_{\mathrm{m}}$ involving two circuit parameters of Fig. 2 can be obtained as

$$C_1 + C_{\mathrm{m}} = \lim_{\omega \to 0} \frac{1}{\mathrm{j}\omega Z_{\mathrm{r}2}(\omega)} = \frac{\lambda_1}{\xi_0}. \tag{14}$$

Finally, a new complex quantity with dimensions of admittance is defined, which can be also expressed as a rational function of $\omega$ as shown below

$$\frac{1}{Z_{\mathrm{r}2}(\omega)} - \mathrm{j}\omega(C_1 + C_{\mathrm{m}}) = \frac{\mathrm{j}N'''_{\mathrm{o}3}(\omega)}{[\omega^2 + D'''_{\mathrm{e}0}(\omega)] + \mathrm{j}D'''_{\mathrm{o}1}(\omega)}, \tag{15}$$

where $N'''_{\mathrm{o}3}(\omega) = \eta_3\omega^3$, $D'''_{\mathrm{e}0}(\omega) = \varphi_0$ and $D'''_{\mathrm{o}1}(\omega) = \varphi_1\omega$ are real polynomials of the real variable $\omega$. As in previous cases, the TLS method is employed to determine the three unknown coefficients $\eta_3$, $\varphi_1$ and $\varphi_0$. These coefficients are related with the circuit parameters of Fig. 2 by means of the equations

$$\eta_3 = -\frac{C_{\mathrm{m}}^2}{C_2 + C_{\mathrm{m}}} \tag{16}$$

$$\varphi_1 = -\frac{1}{R_2(C_2 + C_{\mathrm{m}})} \tag{17}$$

$$\varphi_0 = -\frac{1}{L_1(C_2 + C_{\mathrm{m}})}. \tag{18}$$

If we fix the value of $R_2$ (in this paper, we have always chosen $R_2 = 50\ \Omega$, which is the usual choice for the load impedance in microwave circuits), then we can use (16) to (18) to solve for $C_1$, $C_2$, $C_{\mathrm{m}}$ and $L_2$ in terms of $R_2$, $\eta_3$, $\varphi_1$, $\varphi_0$, $\lambda_1$ and $\xi_0$ as shown below

$$C_1 = \frac{\lambda_1}{\xi_0} - \sqrt{\frac{\eta_3}{\varphi_1 R_2}} \tag{19}$$

$$C_2 = -\frac{1}{\varphi_1 R_2} - \sqrt{\frac{\eta_3}{\varphi_1 R_2}} \tag{20}$$

$$C_{\mathrm{m}} = \sqrt{\frac{\eta_3}{\varphi_1 R_2}} \tag{21}$$

$$L_2 = R_2 \frac{\varphi_1}{\varphi_0}. \tag{22}$$

TABLE I
ANTENNA SUBSTRATE LAYERS PARAMETERS AS SHOWN IN FIG. 1(A).

| Layer number | $h_i$ (mm) | $\varepsilon_{r,i}$ | $\tan\delta_i$ |
|---|---|---|---|
| $i = 1$ | 1.575 | 2.2 | 0.0009 |
| $i = 2$ | 1.575 | 2.2 | 0.0009 |
| $i = 3$ | 4.8 | 1.06 | 0.0001 |
| $i = 4$ | 0.254 | 2.2 | 0.0009 |

TABLE II
ANTENNA GEOMETRICAL PARAMETERS (IN MM) AS SHOWN IN FIGS. 1(B) TO (E).

| $l_1$ | $w_1$ | $l_2$ | $w_2$ | $s_2$ | $l_3$ | $w_3$ | $s_3$ |
|---|---|---|---|---|---|---|---|
| 9.69 | 4.9 | 4.65 | 12.8 | 1.4 | 15.5 | 17 | 0.5 |
| $a_3$ | $b_3$ | $c_3$ | $d_3$ | $e_3$ | $g_3$ | $l_4$ | $w_4$ |
| 2.5 | 0.5 | 13.6 | 7.5 | 0.5 | 0.5 | 17.5 | 18.4 |

The approach described for the determination of the lumped elements parameters of Fig. 2 has been applied to the case where the substrate and geometrical parameters of the antenna of Fig. 1 are those shown in Tables I and II. In Fig. 3 the results obtained for the real and imaginary part of $Z_{\mathrm{in}}(\omega)$ with Momentum simulations (solid lines) are compared with those obtained with the equivalent circuit of Fig. 2 after application of (2) to (22) (dashed lines). Although the agreement between the two sets of results is not excellent, the EC parameters obtained with plain application of TLS (see first row of Table III) provide a very reasonable approximation of the input impedance frequency response. In order to refine the EC obtained, we have introduced the lumped element parameters obtained with plain TLS in a gradient optimization routine of ADS commercial software [34], and we have optimized the values of $L_1$, $C_1$, $C_2$, $C_{\mathrm{m}}$ and $L_2$ to match Momentum simulations of the input impedance with the EC response. After a few optimization runs, we have obtained new lumped element parameters that exactly match the real and imaginary parts of $Z_{\mathrm{in}}(\omega)$ as shown in Fig. 3. The EC parameters obtained after optimization are those shown in second row of Table III. Please note that the optimized lumped element parameters in Table III differ from the original lumped element parameters obtained with plain TLS by less than 10%. We have carried out many estimations of ECs of antennas of the type shown in Fig. 1, and the optimized EC parameters never differed from the original TLS parameters by more than 15%. This means that although the method presented in this subsection for the estimation of EC parameters is not exact, it provides an excellent starting point for an optimization routine that leads to the exact solution. And the whole process leading to the final optimized solution only takes a few seconds of CPU time in a

laptop computer. Note this strategy can be applied not only to the EC of Fig. 2, but also can be extended to more sophisticated ECs of other different antennas.

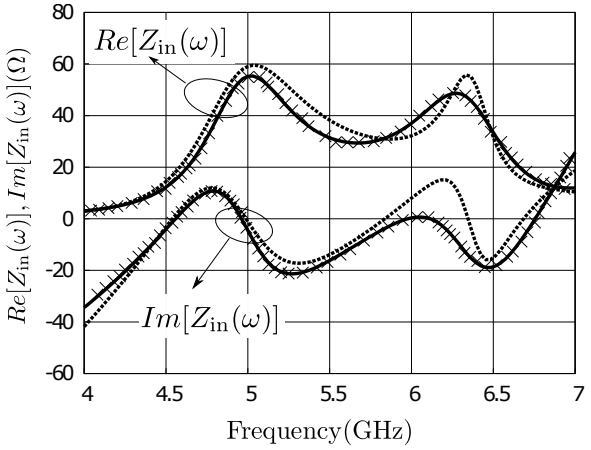


Fig. 3. $\mathrm{Re}[Z_{\rm in}](\omega)$ and $\mathrm{Im}[Z_{\rm in}](\omega)$ (in ohms) for the aperture-coupled stacked microstrip antenna of Fig. 1. Momentum simulations (solid lines) are compared with the results provided by the EC of Fig. 2 after de-embedding of EC parameters with four TLS iterations (dashed lines), and with the results provided by the same EC after optimization of the TLS results ($\times$).

TABLE III
EC PARAMETERS OF FIG. 2 FOR THE ANTENNA OF FIG. 1 WITH SUBSTRATE AND GEOMETRICAL PARAMETERS GIVEN BY TABLES I AND II.

| Numerical method | $L_0$ (nH) | $C_0$ (pF) | $L_1$ (nH) | $C_1$ (pF) | $C_{\rm m}$ (pF) | $L_2$ (nH) | $C_2$ (pF) |
|---|---|---|---|---|---|---|---|
| Plain TLS | 0.312 | 2.56 | 0.354 | 1.69 | 0.690 | 0.390 | 1.64 |
| Optim. TLS | 0.312 | 2.56 | 0.370 | 1.56 | 0.770 | 0.370 | 1.56 |

### *C. Second-order filters for broadband antenna design*

In this paper we intend to design the stage of Fig. 2 consisting of two capacitively coupled parallel LC resonators (right half of the EC of Fig. 2) as a broadband second-order bandpass filter in order to achieve broadband matching for the antenna of Fig. 1. As commented above, the LC series resonator existing between the filtering stage and the input transmission line stands for the feeding mechanism of the antenna (stub+aperture), and will be used to match the filtering stage to the transmission line.

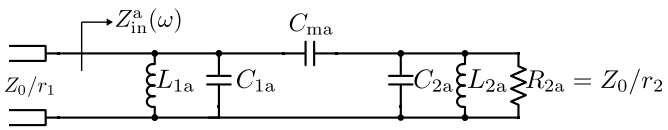


Fig. 4. Classic second-order coupled resonator filter with capacitive coupling between resonators.

Fig. 4 shows the topology of a classic second-order bandpass filter made of capacitively coupled resonators. Let $f_0 = \omega_0/2\pi$ be the center frequency of operation, let $\Delta$ be the fractional bandwidth, and let $Z_0/r_1$ be the impedance of the input transmission line (in practice, we will use $Z_0 = 50\ \Omega$ and $r_1 = 1$ as is customarily done in microwave engineering). Also, let $q_1$ and $q_2$ be the normalized loaded quality factors of the resonators, let $k_{12}$ be the normalized coupling coefficient between the two resonators, and let $r_1$ and $r_2$ be the normalized load admittances. The dimensionless parameters $q_1$, $q_2$, $k_{12}$, $r_1$ and $r_2$ are determined by the desired frequency response of the second-order filter (Butterworth, Chebyshev, maximally flat delay, linear phase equiripple, Gaussian, etc.), and can be found in [35, Table I] for different types of filters. According to the classical theory of filter synthesis, the lumped element parameters of the second-order filter of Fig. 4 can be obtained in terms of $\Delta$, $\omega_0$, $Z_0$, $q_1$, $q_2$, $k_{12}$, $r_1$ and $r_2$ as shown below [36, Chapter 6]

$$L_{1\rm a} = \frac{Z_0\Delta}{\omega_0 q_1 r_1} \tag{23}$$

$$C_{1\rm a} = \frac{q_1 r_1}{\omega_0 Z_0 \Delta}\left[1 - \Delta k_{12}\sqrt{\frac{q_2 r_2}{q_1 r_1}}\right] \tag{24}$$

$$C_{\rm ma} = \frac{k_{12}}{\omega_0 Z_0}\sqrt{q_1 q_2 r_1 r_2} \tag{25}$$

$$L_{2\rm a} = \frac{Z_0\Delta}{\omega_0 q_2 r_2} \tag{26}$$

$$C_{2\rm a} = \frac{q_2 r_2}{\omega_0 Z_0 \Delta}\left[1 - \Delta k_{12}\sqrt{\frac{q_1 r_1}{q_2 r_2}}\right] \tag{27}$$

Based on the topology of Fig. 4, let us assume we want to design a Chebyshev filter with 0.5 dB ripple, a center frequency of 5.57 GHz and a fractional bandwidth of 30%. This filter should be a good candidate for the filtering stage of the antenna EC of Fig. 2 since it ensures a maximum value for $|S_{11}|$ of -9.64 dB in the neighborhood of the center frequency, which roughly coincides with the -10 dB limit customarily employed for antenna impedance matching. Taking into account the specifications, using the fourth row of [35, Table I] and using Eqns. (23) to (27), we finally obtain the lumped element parameters shown in Table IV. Note the resulting filtering circuit is rather asymmetric. First, the inductances and capacitances of the LC parallel resonators are very different. Second, the output load impedance is nearly half the input load impedance. These asymmetries turn out to have a deleterious effect on the use of this filter circuit for the design of the antenna of Fig. 1 by means of the EC of Fig. 2. In fact, we have not been able to match the lumped element values of Table IV with the method of subsection II.B by adjusting the substrate and geometrical parameters of the antenna. One possible way to introduce symmetry in the lumped element values of the second-order filter would be to use a Butterworth configuration with the same values of $f_0$ and $\Delta$. However, in the Butterworth configuration the two reflection zeros are coincident or nearly coincident, and the two reflection zeros of broadband microstrip antennas made of coupled resonators are appreciably separated from the center frequency (usually more than 10%) as can be verified in [37, Chapter 7]. Therefore, the Butterworth configuration is useless

for broadband microstrip antenna design, and we have to rely on the Chebyshev configuration.

TABLE IV
LUMPED ELEMENT PARAMETERS OF THE CIRCUIT OF FIG. 4 FOR A CHEBYSHEV RESPONSE WITH 0.5 DB RIPPLE, CENTER FREQUENCY OF 5.57 GHZ, FRACTIONAL BANDWIDTH OF 30%, AND $Z_0/r_1 = 50\ \Omega$.

| $L_{1a}$ (nH) | $C_{1a}$ (pF) | $C_{ma}$ (pF) | $L_{2a}$ (nH) | $C_{2a}$ (pF) | $R_{2a}$ ($\Omega$) |
|---|---|---|---|---|---|
| 0.312 | 1.54 | 1.15 | 0.157 | 4.18 | 25.2 |

Fig. 5(a) shows the second-order filter topology provided by the classic insertion loss method [30, Section 8.3]. Although this topology does not fit the filtering stage of the antenna EC shown in Fig. 2, in the following we will transform the Chebyshev version of this topology into a second-order filter topology of the type shown in Fig. 4 with symmetric arrangement of the lumped elements and response of Chebyshev type. In Section III, we will see this latter filter topology will enable the broadband design of the antenna of Fig. 1 based on filter theory.

For the specific bandpass filter of Fig. 5(a), let $A(\mathrm{dB})$ be the maximum prescribed value of $|S_{11}|$ in decibels in the neighborhood of the center frequency $f_0$ (e. g., if the filter is intended to be used for antenna matching, $A(\mathrm{dB})$ can be chosen around -10 dB). Let us define a dimensionless parameter $K$ in terms of $A(\mathrm{dB})$ as

$$K = \sqrt{\frac{10^{(A(\mathrm{dB})/10)}}{1-10^{(A(\mathrm{dB})/10)}}} \tag{28}$$

If we want that the filter of Fig. 5(a) shows a Chebyshev response with a value of $K$ given by (28), with a fractional bandwidth $\Delta$ and input impedance $Z_0$, the lumped element parameters $R_\mathrm{L}$, $L_\mathrm{I}$, $C_\mathrm{I}$, $L_\mathrm{II}$, and $C_\mathrm{II}$ of Fig. 5(a) must be obtained in terms of $\Delta$, $\omega_0$, $Z_0$ and $K$ as shown below [30]

$$R_\mathrm{L} = Z_0\left[1+2K^2-2K\sqrt{1+K^2}\right] \tag{29}$$

$$L_\mathrm{I} = \frac{Z_0\Delta\left[\sqrt{R_\mathrm{L}Z_0}-2KR_\mathrm{L}\right]^{1/2}}{2\omega_0\sqrt{KR_\mathrm{L}}} \tag{30}$$

$$C_\mathrm{I} = \frac{2\sqrt{KR_\mathrm{L}}}{\omega_0 Z_0\Delta\left[\sqrt{R_\mathrm{L}Z_0}-2KR_\mathrm{L}\right]^{1/2}} \tag{31}$$

$$L_\mathrm{II} = \frac{2\sqrt{KZ_0}\left[\sqrt{R_\mathrm{L}Z_0}-2KR_\mathrm{L}\right]^{1/2}}{\omega_0\Delta} \tag{32}$$

$$C_\mathrm{II} = \frac{\Delta}{2\omega_0\sqrt{KZ_0}\left[\sqrt{R_\mathrm{L}Z_0}-2KR_\mathrm{L}\right]^{1/2}} \tag{33}$$

Now, let us focus on the series association of the inductance $L_\mathrm{II}$ and the resistance $R_\mathrm{L}$ at the right side of the circuit of Fig. 5(a). If $R_\mathrm{L} << \omega_0 L_\mathrm{II}$, which is a condition always fulfilled for narrow bandwidth filters and approximately fulfilled for moderate and wide bandwidth filters, in the neighborhood of $f_0$ the series association $L_\mathrm{II}-R_\mathrm{L}$ can be approximated by the parallel association of the inductance $L_\mathrm{II}$ and the resistance $R_\mathrm{Lm}$ shown in Fig. 5(b), where $R_\mathrm{Lm}$ is defined as

$$R_\mathrm{Lm} = \frac{(\omega_0 L_\mathrm{II})^2}{R_\mathrm{L}} \tag{34}$$

When the $L_\mathrm{II}-R_\mathrm{L}$ series circuit located at the right side of the circuit of Fig. 5(a) is substituted by the approximate $L_\mathrm{II}-R_\mathrm{Lm}$ parallel circuit of Fig. 5(b), one obtains a new circuit with a slightly different electrical response since the resulting topology is only an approximation of the original topology. For a Chebyshev filter with $A(\mathrm{dB})$=-11 dB, a center frequency of 5.57 GHz and a fractional bandwidth of 30%, the solid line of Fig. 6 shows the reflection coefficient obtained with the insertion loss method filter of Fig. 5(a), and the dashed line shows the reflection coefficient obtained when the transformation of Fig. 5(b) is introduced in Fig. 5(a). Note that the responses of the two circuits are not very different except for the fact that the two reflection zeros of the original filter of Fig. 5(a) have been smoothed after the transformation. Bearing in mind that the responses are not very different, we have used the gradient optimization facility of ADS commercial software [34] to optimize the values of $L_\mathrm{I}$, $C_\mathrm{I}$, $L_\mathrm{II}$, $C_\mathrm{II}$ and $R_\mathrm{Lm}$ in the transformed circuit so that the values of $|S_{11}|$ match the two reflection zeros and the maximum in the neighborhood of $f_0$ (for which $A(\mathrm{dB})$=-11 dB) in the original filter. After a few seconds of CPU time in a laptop computer, we have obtained an optimized circuit that completely matches the response of the circuit of Fig. 5(a) as shown in Fig. 6. This new optimized circuit is drawn in Fig. 5(c), and we insist on the fact that its electrical response is identical to that of the filter of Fig. 5(a). Table V shows the lumped element parameters obtained for the circuits of Figs. 5(a) and (c) to obtain the response of Fig. 6. Please note that the optimization process has changed the values of $L_\mathrm{I}$, $C_\mathrm{I}$, $L_\mathrm{II}$, $C_\mathrm{II}$ and $R_\mathrm{Lm}$ by less than 10% (the value of $R_\mathrm{Lm}$ before optimization was $421.5\ \Omega$). As it happens with the optimization carried out to obtain the results of Fig. 3, the starting point used for the optimization leading to Fig. 6 is again very close to the final solution, and therefore, the optimization process requires tiny computational resources.

TABLE V
LUMPED ELEMENT PARAMETERS OF THE CIRCUITS OF FIGS. 5(A) AND (C) FOR A CHEBYSHEV RESPONSE WITH $A(\mathrm{dB})$=-11 DB, $f_0 = 5.57$ GHZ, $\Delta = 0.3$ AND $Z_0 = 50\ \Omega$.

| $L_\mathrm{I}$ (nH) | $C_\mathrm{I}$ (pF) | $L_\mathrm{II}$ (nH) | $C_\mathrm{II}$ (pF) | $R_\mathrm{L}$ ($\Omega$) |
|---|---|---|---|---|
| 0.368 | 2.21 | 3.10 | 0.262 | 28.0 |
| $L_\mathrm{I}^\mathrm{opt}$ (nH) | $C_\mathrm{I}^\mathrm{opt}$ (pF) | $L_\mathrm{II}^\mathrm{opt}$ (nH) | $C_\mathrm{II}^\mathrm{opt}$ (pF) | $R_\mathrm{Lm}^\mathrm{opt}$ ($\Omega$) |
| 0.359 | 2.14 | 3.35 | 0.257 | 463 |

The reason why we have obtained the circuit of Fig. 5(c) from the circuit of Fig. 5(a) is because this circuit is a minimum impedance representation of the circuit of Fig. 4 [38], i. e., there exists a circuit with the topology of Fig. 4 with exactly

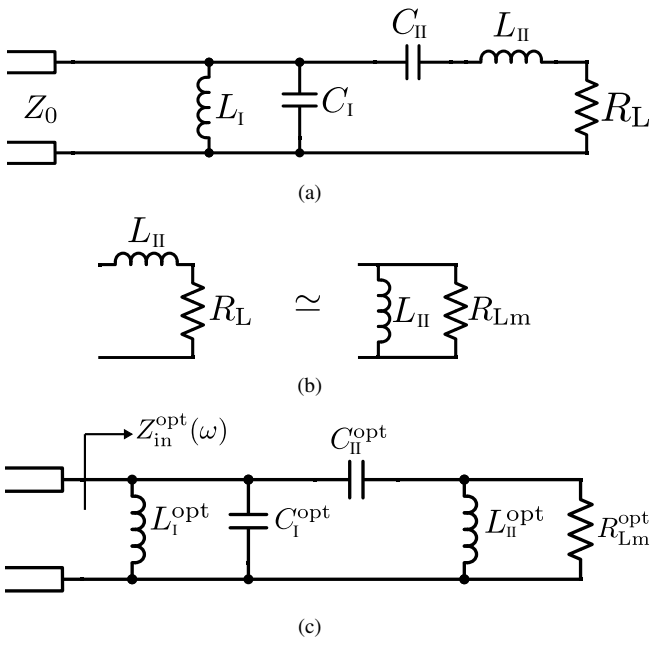


Fig. 5. (a) Classic second-order bandpass filter based on the insertion loss method. (b) Approximate transformation of the series $R_{\rm L} - L_{\rm II}$ circuit into the parallel $R_{\rm Lm} - L_{\rm II}$ circuit when $\omega_0 L_{\rm II} << R_{\rm L}$. (c) Circuit obtained when the approximation of Fig. 5(b) is introduced in Fig. 5(a), and the resulting circuit is optimized to match the response of the circuit of Fig. 5(a).

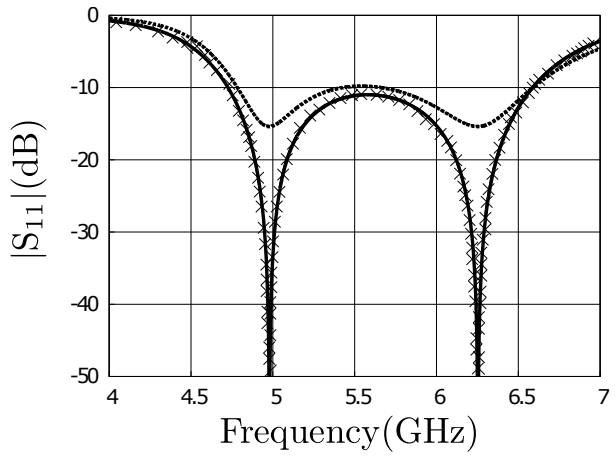


Fig. 6. Reflection coefficient for the circuit of Fig. 5(a) (solid line), for the circuit obtained when the approximation of Fig. 5(b) is introduced in Fig. 5(a) (dashed line), and for this latter circuit after optimization -i.e., for the circuits of Figs. 5(c) and 7- ($\times$).

the same input impedance as that of the circuit of Fig. 5(c), and therefore, with the same electrical response of the circuit of Fig. 5(a) according to Fig. 6. The circuit with the topology of Fig. 4 which is equivalent to the circuit of Fig. 5(c) has been represented in Fig. 7, which means that $Z_{\rm in}^{\rm opt}(\omega) = Z_{\rm in}^{\rm b}(\omega)$. If the mathematical procedures described in [38] are employed, it is possible to show that once the value of the load impedance in Fig. 7, $R_{2\rm b}$, is arbitrarily chosen (e. g., $R_{2\rm b}$ can be taken to be 50 $\Omega$ as is customarily done in microwave circuits), $L_{1\rm b}$, $C_{1\rm b}$, $C_{\rm mb}$, $L_{2\rm b}$ and $C_{2\rm b}$ can be defined in terms of $L_{\rm I}^{\rm opt}$, $C_{\rm I}^{\rm opt}$, $L_{\rm II}^{\rm opt}$, $C_{\rm II}^{\rm opt}$, $R_{\rm Lm}^{\rm opt}$ and $R_{2\rm b}$ as shown below

$$L_{1\rm b} = L_{\rm I}^{\rm opt} \tag{35}$$

$$C_{1\rm b} = C_{\rm I}^{\rm opt} - C_{\rm II}^{\rm opt}\left[\sqrt{\frac{R_{\rm Lm}^{\rm opt}}{R_{2\rm b}}} - 1\right] \tag{36}$$

$$C_{\rm mb} = C_{\rm II}^{\rm opt}\sqrt{\frac{R_{\rm Lm}^{\rm opt}}{R_{2\rm b}}} \tag{37}$$

$$L_{2\rm b} = \frac{R_{2\rm b} L_{\rm II}^{\rm opt}}{R_{\rm Lm}^{\rm opt}} \tag{38}$$

$$C_{2\rm b} = C_{\rm II}^{\rm opt}\sqrt{\frac{R_{\rm Lm}^{\rm opt}}{R_{2\rm b}}}\left[\sqrt{\frac{R_{\rm Lm}^{\rm opt}}{R_{2\rm b}}} - 1\right] \tag{39}$$

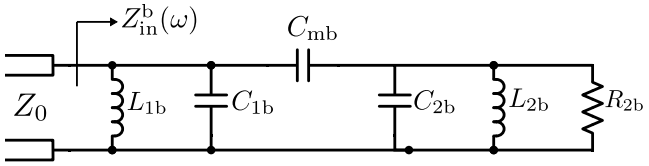


Fig. 7. Circuit containing two capacitively coupled resonators, with exactly the same frequency response as the circuit of Fig. 5(c) ($R_{2\rm b}$ can be arbitrarily chosen).

TABLE VI
LUMPED ELEMENT PARAMETERS OF THE CIRCUIT OF FIG. 7 FOR A CHEBYSHEV RESPONSE WITH $A$(dB)=-11 dB, $f_0 = 5.57$ GHz, $\Delta = 0.3$ AND $Z_0 = 50\ \Omega$.

| $L_{1\rm b}$ (nH) | $C_{1\rm b}$ (pF) | $C_{\rm mb}$ (pF) | $L_{2\rm b}$ (nH) | $C_{2\rm b}$ (pF) | $R_{2\rm b}$ ($\Omega$) |
|---|---|---|---|---|---|
| 0.370 | 1.56 | 0.770 | 0.370 | 1.56 | 50 |

Table VI shows the lumped element parameters of the circuit of Fig. 7 that provide the frequency response of the solid line of Fig. 6. Please compare Table VI with Table IV. Whereas the circuit corresponding to Fig. 4 and Table IV is very asymmetric, the circuit corresponding to Fig. 7 and Table VI is completely symmetric since it contains equal LC parallel resonators and equal load impedances. Also, both circuits show very similar Chebyshev responses as shown in Fig. 8. Since the circuit of Fig. 7 fits with the antenna EC of Fig. 2, this circuit will be used in the next section to design the broadband microstrip antenna of Fig. 1. Owing to the symmetry of the circuit described by Fig. 7 and Table VI, the lumped parameters of Table VI are feasible to obtain by conveniently adjusting the substrate and geometrical parameters of the antenna.

To be strictly honest, after optimization and application of (35) to (39) to derive the lumped element parameters of Fig. 7, we did not exactly obtain equal values for $L_{1\rm b}$ and $L_{2\rm b}$, and for $C_{1\rm b}$ and $C_{2\rm b}$, as it appears in Table VI. However, the differences observed between $L_{1\rm b}$ and $L_{2\rm b}$, and between $C_{1\rm b}$ and $C_{2\rm b}$, were smaller than 1%. So, we took the arithmetic mean of the resulting values for $L_{1\rm b} = L_{2\rm b}$ and for $C_{1\rm b} = C_{2\rm b}$, and we did not observe any appreciable change in the frequency response of the circuit.

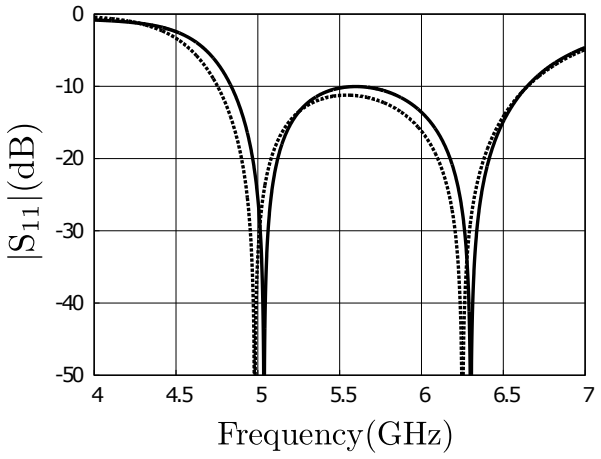


Fig. 8. Reflection coefficient for the circuit of Fig. 4 and Table IV (solid line), and for the circuit of Fig. 7 and Table VI (dashed line).

The strategy followed to derive the circuit of Fig. 7 from the circuit of Fig. 5(a) has been applied for other center frequencies and other fractional bandwidths, and the final result has always been a symmetric circuit with the topology of Fig. 7 and Chebyshev response. This means the design methodology described in this subsection can be equally extended to different center frequencies and different fractional bandwidths.

### *D. Antenna design tips and parametric studies*

The filtering stage used in Fig. 2 for the antenna designed in this paper is that shown in Fig. 7 with circuit parameters given by Table VI. These circuit parameters are reproduced in the row of Optimized TLS values of Table III, which provides the lumped element values of the complete EC for the antenna designed in the paper. The substrate and geometrical parameters of the antenna have to be adjusted so as to match these circuit parameters. The most critical parameters in the adjustment process are the coupling capacitance, $C_{\mathrm{m}}$, and the inductance of the lower patch, $L_1$.

Bottom up, the first two layers of Fig. 1(a) have been chosen to be Rogers RT/Duroid of thickness 62 mils -1.575 mm-, the third layer is made of Cumin Microwave C-Foam PF-4, and the fourth layer is Rogers RT/Duroid of thickness 10 mils -0.254 mm- (the relative permittivity and loss tangents of these materials are provided in Table I). The thickness of the C-Foam layer $h_3$ is crucial to adjust the coupling capacitance $C_{\mathrm{m}}$ of Fig. 2. In order to estimate this thickness, the two patches of Fig. 1 are substituted by two square patches with lengths $l_3$ and $l_4$ equal to half a wavelength at the center frequency of the antenna ($f_0 = 5.57$ GHz in our design). Since the thickness of the C-Foam is commercially available in multiples of 1.6 mm, we select the value of $h_3$ that leads to a value of $C_{\mathrm{m}}$ which is closest to the target value $C_{\mathrm{m}} = 0.77$ pF. Fig. 9 shows the values of $C_{\mathrm{m}}$ as a function of $h_3$ when all the parameters in the antenna finally designed are kept fixed (see Tables I and II) except for $h_3$. Please note that $C_{\mathrm{m}}$ strongly depends on $h_3$, and that variations within 50% are obtained in the values of $C_{\mathrm{m}}$ as $h_3$ changes from 3.2 mm to 6.4 mm. In this case, a value of $h_3 = 4.8$ mm matches the required value $C_{\mathrm{m}} = 0.77$ pF.

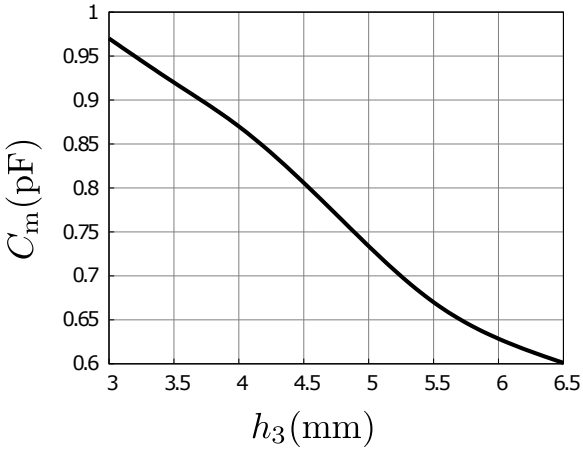


Fig. 9. Coupling capacitance $C_{\mathrm{m}}$ of Fig. 2 as a function of the foam layer thickness $h_3$ in Fig. 1(a). Except for $h_3$, the rest of the antenna substrate and geometrical parameters are kept as shown in Tables I and II.

Once the value of $C_{\mathrm{m}}$ has been fixed, we focus on matching the inductance of the lower patch $L_1$ in Fig. 2. This inductance can be modified by varying the width $w_3$ of the resonant square patch mentioned in the previous paragraph, but the resulting values turn out to be always below the target inductance $L_1$ =0.37 nH required in Table III. And this is important because the circuit model is telling us that we cannot reach the desired goal if we use a lower patch of rectangular shape. Therefore, in order to increase the inductance of the lower patch, we have introduced inner slots close to the center of the patch and meandering slots close to the corners of the patch as shown in Fig. 1(c). These slots reduce the width of the current paths on the patch surface, thus increasing the inductance. By carefully adjusting the length of the inner slots, $a_3$, and the separation of the inner slots, $e_3$, it is possible to match the inductance of the patch to the desired value. Fig. 10 shows that changes in the value of $a_3$ make it possible a tuning of the inductance within 7% when all other antenna parameters are kept fixed. An additional tuning of the inductance can be achieved by adjusting $e_3$.

When the values of $C_{\mathrm{m}}$ and $L_1$ are fixed, we have checked that variations in the width $w_4$ of the upper patch do suffice to achieve the target inductance $L_2 = 0.37$ nH, i. e., the required inductance can be achieved by using an upper patch of rectangular shape. Once the values of $C_{\mathrm{m}}$, $L_1$ and $L_2$ have been adjusted by means of $h_3$, $a_3$, $e_3$ and $w_4$, slight variations of $l_3$ and $l_4$ are needed for a fine adjustment of $C_1$ and $C_2$, which depend on the resonant length of the patches for fixed values of $L_1$ and $L_2$.

As commented above, the circuit parameters $L_0$ and $C_0$ of Fig. 2 have been adjusted by means of $l_1$, $l_2$ and $w_2$ (see Figs. 1(d) and (e)) so as to ensure a good matching between the feeding line and the filtering stage in the whole frequency band where $|S_{11}| <$ -10 dB for the filtering stage (i.e., roughly the band between 4.8 and 6.6 GHz in Fig. 6). The final circuit

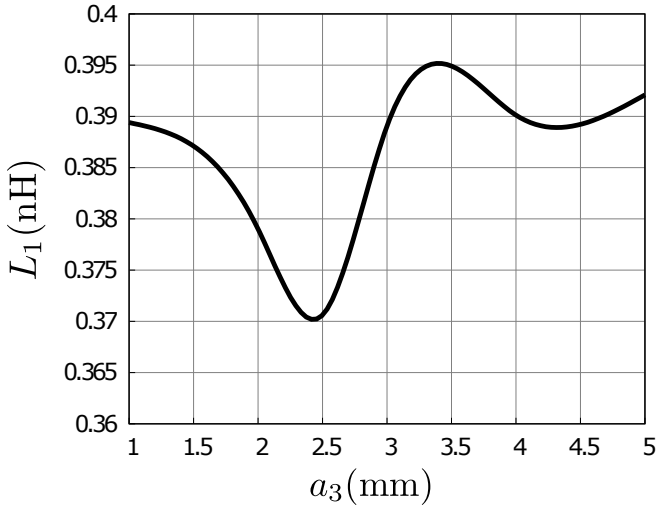


Fig. 10. Lower patch inductance $L_1$ of Fig. 2 as a function of the length of the meandering slots $a_3$ in Fig. 1(c). Except for $a_3$, the rest of the antenna substrate and geometrical parameters are kept as shown in Tables I and II.

parameters of the complete EC for the designed antenna are those shown in Table III, and the final substrate and antenna parameters corresponding to this EC are those shown in Tables I and II.

## III. Numerical and Experimental Results

The broadband microstrip antenna of Fig. 1 with substrate and geometrical parameters shown in Tables I and II, which is characterized by the EC of Fig. 1 with circuit parameters given by Table III, has been fabricated and measured. Fig. 11(a) shows a photograph the antenna mounted in the anechoic chamber, and Figs. 11(b) to (e) shows photographs of the different metallization levels. As shown in Fig. 11(a), plastic screws are used to join the three RT/Duroid layers and the foam layer. The upper patch is printed on the back side of the 10 mils upper RT/Duroid layer, the lower patch is printed on the front side of one of the 62 mils Duroid layers, and the feeding strip, on the back side of the other 62 mils Duroid layer.

Fig. 12 shows the comparison between simulated and measured results for the reflection coefficient of the antenna of Fig. 11. Note that the impedance matching fractional bandwidth for $|S_{11}|$ < -10 dB is roughly 32% (between 4.69 and 6.52 GHz) in the case of the simulated antenna with parameters chosen as in Tables I and II (black dashed line), and that the fractional bandwidth is roughly 33% (between 4.80 and 6.73 GHz) in the case of the measured antenna (solid line). In both cases, the matching operation band covers the complete band between 4.9 and 6.0 GHz, which includes most WLAN channels of the 802.11 standard and the 5.8 GHz ISM band. There is a shift of roughly 0.2 GHz between the matching simulated band and the matching measured band. This shift is attributed to the fact that the real relative permittivity of RT/Duroid 5880 was slightly smaller than the value provided by the manufacturer, and to the fact that the thickness of the C-foam layer was also smaller than the value provided by the

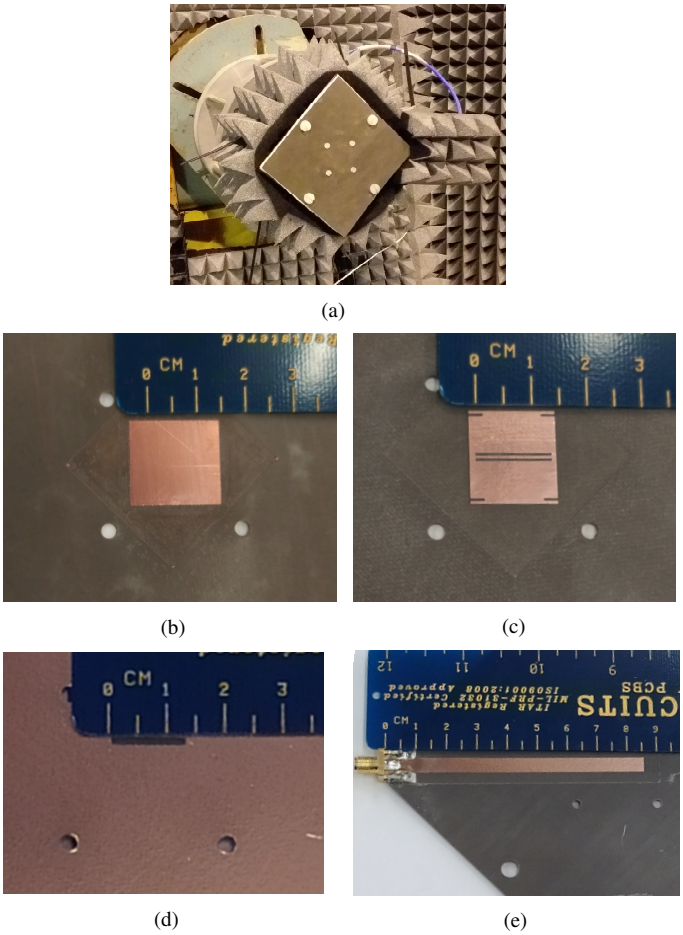


Fig. 11. (a) Photograph of the broadband microstrip antenna in the anechoic chamber. Photographs of the details of the different metallization levels of the antenna: (b) upper patch (metallization level 4); (c) lower patch (metallization level 3); (d) ground plane rectangular aperture (metallization level 2); (e) feeding strip (metallization level 1).

manufacturer (in fact, this smaller thickness was measured). The antenna was simulated once again by assuming that the relative permittivity of RT/Duroid was 2.0 instead of 2.2, and that the thickness of C-Foam was 4.3 mm instead of 4.8 mm. These new simulation results are also included in Fig. 12 (grey dashed line), showing the new simulated matching band for the antenna is between 4.87 and 6.74 GHz, which is much closer to the matching band obtained in the experiments. The closer agreement between simulations with corrected substrate parameters and experiments shows the frequency shift existing between the simulated results with nominal substrate parameters and the experimental results can be satisfactorily explained by overestimated values of RT/Duoid permittivity and C-foam layer thickness.

Fig. 13 shows the comparison between simulated and measured results for the radiation patterns of the antenna of Fig. 11. The simulations have been performed with CST Studio Suite® (CST SS) [39] to account for the effects of the edges of the substrate in the real antenna, which cause diffraction and back radiation. The effects of the substrate truncation cannot be taken into account in the simulations with Momentum software [32], since this software assumes the substrate is of infinite

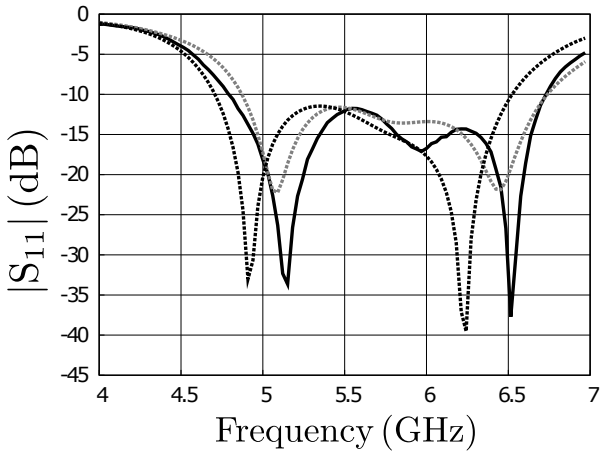


Fig. 12. Reflection coefficient of the designed antenna. Measured values (solid line) are compared with simulated values obtained with the nominal data of Tables I and II (black dashed line), and with simulated values obtained with corrected data for permittivity of Rogers RT/Duroid -$\varepsilon_{r,1} = \varepsilon_{r,2} = \varepsilon_{r,4} = 2.0$- and for thickness of C-Foam layer -$h_3 = 4.3$ mm- (grey dashed line).

extent. Pyramidal microwave absorber was added below the antenna in the CST SS simulations since this absorber was also used in the measurements to mitigate the back radiation (see Fig. 11(a)). The results of Fig. 13 show the radiation pattern is quite stable in the antenna operating frequency band between 5 and 6.5 GHz. Both simulated and measured cross-polarization levels are always below -20 dB. This low cross-polarization is attributed to the fact that the upper patch of Fig. 1(b) has a simple rectangular geometry with negligible currents in the $x$ direction in the neighborhood of the excited resonance. In the lower patch of Fig. 1(c) with inner and meandering slots, the $x$ component of the current is more relevant, but its radiation is shielded by the upper patch. The cross-polarization of the antena would have probably been larger if the positions of the patches of Figs. 1(b) and (c) had been exchanged in the antenna, which shows the advantage of the antenna geometry proposed in Fig. 1 in terms of polarization purity.

In Fig. 14 we compare the simulated and measured values of gain for the antenna of Fig. 11. As in the case of Fig. 12, we provide two different sets of simulated results, one for the antenna with nominal substrate parameters and dimensions as shown in Tables I and II (black dashed line), and one with corrected relative permittivity of Rogers RT/Duroid and corrected thickness of the C-foam layer (grey dashed line). The simulated values of gain have been obtained with CST SS, just as the simulated radiation patterns of Fig. 13. As it happens in Fig. 12, in Fig. 14 the simulated results with corrected substrate parameters are closer to the measured results than the simulated results with nominal substrate parameters. In fact, the measured values of gain lie between 6 and 7 dBi in most of the operating frequency band, which is reasonable for microstrip antennas printed on a low-permittivity substrate [40]. And the simulated values with corrected substrate parameters lie on average around 0.5 dB above these measured values. However, the simulated values with nominal substrate parameters can differ as much as 2 dB from the measured values at the extremes of the operating frequency band.

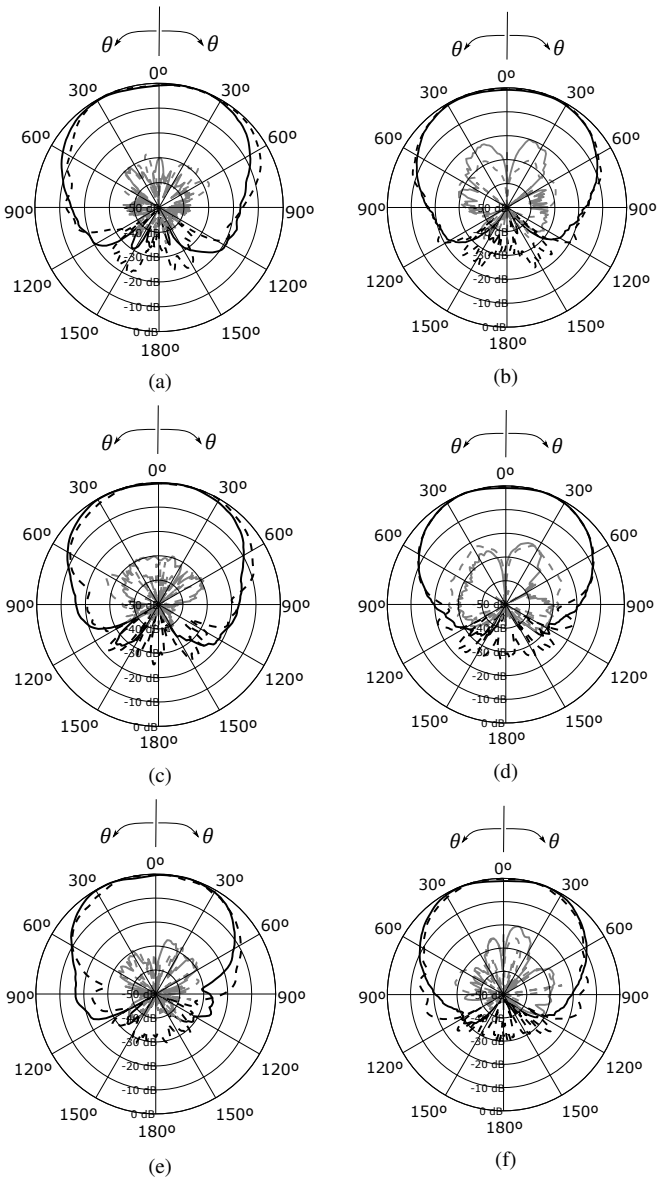


Fig. 13. Co-polar (black) and cross-polar (grey) components of the radiation patterns for the designed antenna. Solid lines stand for measurements, and dashed lines stand for CST SS simulations. (a) E-plane results at 5 GHz. (b) H-plane results at 5 GHz. (c) E-plane results at 5.75 GHz. (d) H-plane results at 5.75 GHz. (e) E-plane results at 6.5 GHz. (f) H-plane results at 6.5 GHz.

## IV. Conclusion

In this paper we present a systematic circuit methodology for the design of broadband microstrip antennas made of two stacked patches fed by an aperture in the ground plane of a microstrip line. An EC is proposed for the antenna, and a novel de-embedding technique for the determination of the parameters of the EC is introduced, which uses an iterative total least squares approach plus slight optimization to yield a perfect matching between the EC response and EM simulations. Then, the geometry of the stacked patches is adjusted so that their EC follows a second order quasi-Chebyshev response

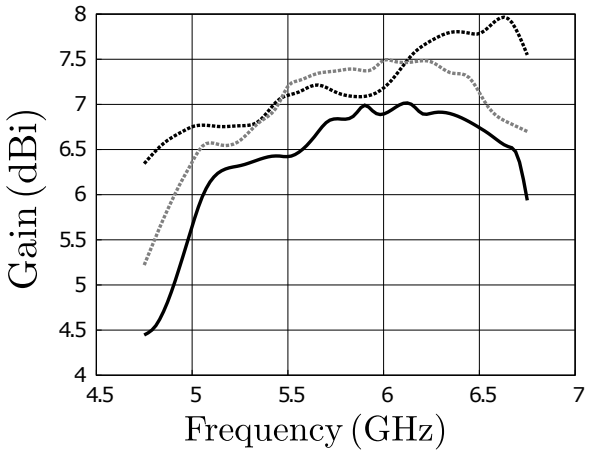


Fig. 14. Gain of the designed antenna. Measured values (solid line) are compared with simulated values obtained with the nominal data of Tables I and II (black dashed line), and with simulated values obtained with corrected data for permittivity of Rogers RT/Duroid -$\varepsilon_{r,1} = \varepsilon_{r,2} = \varepsilon_{r,4} = 2.0$- and for thickness of C-Foam layer -$h_3 = 4.3$ mm- (grey dashed line). The simulations have been performed with CST SS.

derived from the insertion loss method. This quasi-Chebyshev response has the advantage that it is originated by a symmetric circuit which can be physically implemented by means of un upper rectangular patch coupled to a lower rectangular patch with inner and meandering slots. Based on the EC with quasi-Chebyshev response, a stacked patch microstrip antenna has been designed with a 30% of fractional bandwidth at a center frequency of 5.57 GHz. The antenna has been fabricated and measured, and a good agreement has been found between simulations and measurements for the return loss (experimental fractional bandwidth of 33% for $|S_{11}| <$ -10 dB in the measured antenna), for the radiation pattern and for the gain, especially if the nominal substrate parameters are slightly tuned in the simulations to make them closer to the real values used in the experiments.

## REFERENCES


[1] D. M. Pozar, "Microstrip antennas," *Proceedings IEEE*, vol. 80, no. 1, pp. 79-91, Jan. 1992.

[2] D. M. Pozar, "Microstrip antenna aperture-coupled to a microstripline," *Electron. Lett.*, vol. 21, no. 2, pp. 49-50, Jan. 1985.

[3] P. L. Sullivan and D. H. Schaubert, "Analysis of an aperture coupled microstrip antenna," *IEEE Trans. Antennas Propag.*, vol. AP-34, no. 8, pp. 977-984, Aug. 1986.

[4] F. Croq and D. M. Pozar, "Millimeter-wave design of wide-band aperture coupled stacked microstrip antennas," *IEEE Trans. Antennas Propag.*, vol. 39, no. 12, pp. 1770-1776, Dec. 1991.

[5] S. D. Targonsky, R. B. Waterhouse, and D. Pozar, "Design of wide-band aperture-stacked patch microstrip antennas," *IEEE Trans. Antennas Propag.*, vol. 46, no. 9, pp. 1245-1251, Sep. 1991.

[6] M. El Yazidi, M. Himdi, and J. P. Daniel, "Aperture coupled microstrip antenna for dual frequency operation," *Electron. Lett.*, vol. 29, no. 17, pp. 1506-1508, Aug. 1993.

[7] R. Caso, A. A. Serra, M. Rodríguez-Pino, P. Nepa, and G. Manara, "A wideband slot-coupled stacked-patch array for wireless communications," *IEEE Antennas Wireless Propag. Lett.*, vol. 9, pp. 986-989, 2010.

[8] C.-X. Mao, S. Gao, Y. Wang, Q. Luo, and Q.-X. Chu, "A shared-aperture dual-band dual-polarized filtering-antenna-array with improved frequency response," *IEEE Trans. Antennas Propag.*, vol. 65, no. 4, pp. 1836-1844, Apr. 2017.

[9] B. Zhang and Q. Xue, "Filtering antenna with high selectivity using multiple coupling paths from source/load to resonators," *IEEE Trans. Antennas Propag.*, vol. 66, no. 8, pp. 4320-4325, Aug. 2018.

[10] A. I. Abunjaileh, I. C. Hunter, and A. H. Kemp, "Application of dual-mode filter techniques to the broadband matching of microstrip antennas," *IET Microw. Antennas Propag.*, vol. 1, no. 2, pp. 273-276, Apr. 2007.

[11] A. I. Abunjaileh, I. C. Hunter, and A. H. Kemp, "A circuit-theoretic approach to the design of quadruple-mode broadband microstrip patch antennas," *IEEE Trans. Microwave Theory Tech.*, vol. 56, no. 4, pp. 896-900, Apr. 2008.

[12] C.-T. Chuang and S.-J. Chung, "Synthesis and design of a new printed filtering antenna," *IEEE Trans. Antennas Propag.*, vol. 59, no. 3, pp. 1036-1042, Mar. 2011.

[13] W.-J. Wu, Y.-Z. Yin, S.-L. Zuo, Z.-Y. Zhang, and J.-J. Xie, "A new compact filter-antenna for modern wireless communication systems," *IEEE Antennas Wireless Propag. Lett.*, vol. 10, pp. 1131-1134, 2011.

[14] C. X. Mao, S. Gao, Y. Wang, B. Sanz-Izquierdo, Z. Wang, F. Qin, Q. X. Chu, J. Li, G. Wei, and J. Xu, "Dual-band patch antenna with filtering performance and harmonic suppression," *IEEE Trans. Antennas Propag.*, vol. 64, no. 9, pp. 4074-4077, Sep. 2016.

[15] H.-W. Deng, T. Xu, and F. Liu, "Broadband pattern reconfigurable filtering microstrip antenna with Quasi-Yagi structure," *IEEE Antennas Wireless Propag. Lett.*, vol. 17, no. 7, pp. 1127-1131, 2017.

[16] C. X. Mao, Y. Zhang, X. Y. Zhang, P. Xiao, Y. Wang, and S. Gao, "Filtering antennas," *IEEE Microwave Magazine*, vol. 22, no. 11, pp. 52-63, Nov. 2021.

[17] J.-S. Hong, *Microstrip Filters for RF/Microwave Applications*, 2nd. edition. Hoboken, New Jersey: Wiley, 2011, ch. 7.

[18] C.-K. Lin and S.-J. Chung, "A filtering microstrip antenna array," *IEEE Trans. Microwave Theory Tech.*, vol. 59, no. 11, pp. 2856-2863, Nov. 2011.

[19] Q.-S. Wu, L. Zhu, and X. Zhang, "Filtering patch antenna on $\lambda/4$-resonator filtering topology: synthesis design and implementation," IET Microw. Antennas Propag., vol. 11, no. 5, pp. 2241-2246, 2017. doi:10.1049/iet-map.2017.0354.

[20] Q.-S. Wu, X. Zhang, and L. Zhu, "A wideband circularly polarized patch antenna with enhanced axial ratio bandwidth via co-design of feeding network," *IEEE Trans. Antennas Propag.*, vol. 66, no. 10, pp. 4996-5003, Oct. 2018.

[21] C.-K. Lin and S.-J. Chung, "A compact filtering microstrip antenna with quasi-elliptic broadside antenna gain response," *IEEE Antennas Wireless Propag. Lett.*, vol. 10, pp. 381-384, 2011.

[22] H.-T. Hu, F.-C. Chen, J.-F. Kiang, and Q.-X. Chu, "A differential filtering microstrip antenna array with intrinsic common-mode rejection," *IEEE Trans. Antennas Propag.*, vol. 65, no. 12, pp. 7361-7365, Dec. 2017.

[23] S. Amari, F. Seyfert, and M. Bekheit, "Theory of coupled resonator microwave bandpass filters of arbitrary bandwidth," *IEEE Trans. Microwave Theory Tech.*, vol. 58, no. 8, pp. 2188-2203, Aug. 2010.

[24] W. Duan, X. Y. Zhang, Y.-M. Pan, J.-X. Xu, and Q. Xue, "Dual-polarized filtering antenna with high selectivity and low cross-polarization,", *IEEE Trans. Antennas Propag.*, vol. 64, no. 10, pp. 4188-4195, Oct. 2016.

[25] X. Y. Zhang, Y. Zhang, Y.-M. Pan, and W. Duan "Low-profile dual-band filtering patch antenna and its application to LTE MIMO system,", *IEEE Trans. Antennas Propag.*, vol. 65, no. 1, pp. 103-113, Jan. 2017.

[26] K. Dhwaj, L. J. Jiang, and T. Itoh, "Dual-band filtering antenna with novel transmission zero characteristics,", *IEEE Antennas Wireless Propag. Lett.*, vol. 17, no. 12, pp. 2469-2473, Dec. 2018.

[27] R. B. Waterhouse, *Microstrip patch antennas: a designer's guide*. Norwell, Massachussets: Kluwer Academic Publishers, 2003, ch. 3.

[28] J. Rahman and T. K. Sarkar, "Deconvolution and total least squares in finding the impulse response of an electromagnetic system from measured data," *IEEE Trans. Antennas Propag.*, vol. 43, no. 4, pp. 416-421, Apr. 1995.

[29] R. R. Boix, F. Mesa and F. Medina, "Application of total least squares to the derivation of closed-form Green's functions for planar layered media," *IEEE Trans. Microwave Theory Tech.*, vol. 55, no. 2, pp. 268-280, Feb. 2007.

[30] D. M. Pozar, *Microwave Engineering*, 3rd. edition. Hoboken, New Jersey: Wiley, 2005, ch. 8.

[31] M. Al-Joumayly, S. M. Aguilar, N. Behdad, and S. C. Hagness, "Dual-band miniaturized patch antennas for microwave breast imaging," *IEEE Antennas Wireless Propag. Lett.*, vol. 9, pp. 268-271, 2010.

[32] https://www.keysight.com/en/pc-1887116/momentum-3d-planar-em-simulator. Accessed on Nov. 11th 2021.
[33] F. Costa, A. Monorchio, and G. Manara, "Efficient analysis of frequency-selective surfaces by a simple equivalent-circuit model," *IEEE Antennas Propagat. Magazine*, vol. 54, no. 4, pp. 35-48, Aug. 2012.
[34] https://www.keysight.com/es/en/products/software/pathwave-design-software/pathwave-advanced-design-system.html. Accessed on Nov. 11th 2021.
[35] M. Al-Joumayly and N. Behdad, "A new technique for design of low-profile, second-order, bandpass frequency selective surfaces," *IEEE Trans. Antennas Propag.*, vol. 57, no. 2, pp. 452-459, Feb. 2009.
[36] I. A. Zverev, *Handbook of Filter Synthesis*, New York: Wiley, 1967.
[37] K.-L. Wong, *Compact and Broadband Microstrip Antennas*, New York: Wiley, 2002.
[38] G. C. Themes and J. W. LaPatra, *Introduction to Circuit Synthesis and Design*, New York: McGraw-Hill, 1977.
[39] https://www.3ds.com/products-services/simulia/products/cst-studio-suite/. Accessed on Nov. 11th 2021.
[40] C. A. Balanis, *Antenna theory: analysis and design*, 3rd. edition. Hoboken, New Jersey: Wiley, 2005, ch. 14.

**Nieves García-Alcaide** obtained a bachelor degree in Physics and a Master of Science in Microelectronics, both at the University of Seville, in 2018 and 2021 respectively. In 2019, she got a one year Young Researchers grant financed by EU funds. While enjoying the grant in the Microwaves Group of the University of Seville, she carried out research activities related to the design of microstrip antennas based on classical filter theory. Nowadays, she is working at Alter Technology company, where she performs as a microwave engineer.

**Armando Fernández-Prieto** (S'11-M'14-SM'18) was born in Ceuta, Spain, in September 1981. He received the "Licenciado" and Ph.D. degrees in Physics from "Universidad de Sevilla", Spain, in 2007 and 2013, respectively. He is currently Associate Professor of Electromagnetism with the Department of Electronics and Electromagnetism, University of Seville, and member of the Microwaves Group. His research interests focus on printed passive microwave components and metamaterials. Dr. Fernández-Prieto acts as a reviewer for the IEEE Transactions on Microwave Theory and Techniques, IEEE Microwaves and Wireless Components Letters, IEEE Transactions on Antennas and Propagations and IEEE Access, as well as for many other journals.

**Rafael R. Boix** (M'96) got the "Licenciado" and "Doctor" degrees in Physics from the University of Seville, Spain, in 1985 and 1990 respectively. Since 1986, he has been with the Electronics and Electromagnetism Department, University of Seville, where he became Tenured Professor in 2010. He belongs to the Microwaves Group of the University of Seville. His current research interests are focused on the efficient numerical analysis of periodic planar multilayered structures with applications to the design of frequency selective surface and reflectarray antennas, and on the development of circuit approaches for the synthesis of microstrip antennas with frequency selective response.

**Vicente Losada** was born in São Paulo, Brazil, in February 1969. He got the "Licenciado" and "Doctor" degrees in physics from the "Universidad de Sevilla", Spain, in 1992 and 1997, respectively. He has been an Associate Professor with the Department of Applied Physics I, University of Seville, since 2004. His research interests are focused on the manufacture of printed antennas, and on the near-field and far-field accurate measurement of antennas. He acts as a Reviewer for the IEEE Transactions on Antennas and Propagation.

**Jesús Martel** (M'08–SM'15) got the "Licenciado" and "Doctor" degrees in Physics from the University of Seville, Spain, in 1989 and 1996, respectively. Since 1990, he has performed research activities with the Microwaves Group, University of Seville. He is currently a Professor with the Department of Applied Physics II, University of Seville, Spain, where he was Head of the Department from 2010 to 2018. His current research interests are focused on the design of passive microwave circuits, on microwave measurements, and on the study of the properties of artificial media.

**Francisco Medina** (M'90–SM'01–F'10) was born in Puerto Real (Cádiz, Spain) in 1960. He got the "Licenciado" and "Doctor" degrees, both in Physics, from the "Universidad de Sevilla", Spain, in 1983 and 1987, respectively. He is currently a Professor of Electromagnetism with the Department of Electronics and Electromagnetism, "Universidad de Sevilla", where he is also the Head of the Microwaves Group. His current research interests include analytical and numerical methods for planar structures, anisotropic materials, artificial media modeling and planar microwave circuits. He has published a number of book chapters, journal papers, and conference papers on these topics. He is the Editor in Chief of the International Journal of Microwave and Wireless Technologies.